Int. J. Electron. Commun. (AEÜ) 68 (2014) 534–539

Contents lists available at ScienceDirect

International Journal of Electronics and Communications (AEÜ)

journal homepage: www.elsevier.com/locate/aeue

# Passive localization of mixed sources jointly using MUSIC and sparse signal reconstruction

Ye Tian*, Xiaoying Sun

*College of Communication Engineering, Jilin University, Changchun, Jilin 130022, China*

ARTICLE INFO

*Article history:*
Received 8 July 2013
Accepted 29 December 2013

*Keywords:*
Source localization
Sparse representation
MUSIC
Far-field
Near-field

ABSTRACT

Source localization for mixed far-field and near-field sources is considered. By constructing the second-order statistics domain data of array which is only related to DOA parameters of mixed sources, we obtain the DOA estimation of all sources using the weighted $\ell_1$-norm minimization. And then, we use MUSIC spectral function to distinguish the mixed sources as well as to provide a more accurate DOA estimation of far-field sources. Finally, a mixed overcomplete matrix on the basis of DOA estimation is introduced in the sparse signal representation framework to estimate range parameters. The performance of the proposed method is verified by numerical simulations and is also compared with two existing methods.



## 1. Introduction

Source localization is a problem of great importance in many fields such as radar, sonar, electronic surveillance and seismic exploration [1]. Various high-resolution methods like MUSIC [2] and ESPRIT [3] have been proposed to obtain the direction-of-arrival estimation of far-field sources in the past decades. When the sources are located at the near-field region, several efficient methods such as the two-dimensional (2-D) MUSIC [4], the high-order ESPRIT [5] and the path following method [6] are also available.

In some practical applications, such as speaker localization using microphone arrays [7] and guidance (homing) systems [8], both far-field and near-field sources may be encountered. In this case, all the methods above may not be expected to give satisfactory results since they will mismatch the signal model. By constructing two special cumulant matrices, Liang et al. [9] have developed a two-stage MUSIC method for locating mixed sources. Instead of using cumulant, He et al. [10] present a new approach by efficiently using the second-order statistics based MUSIC method. Recently, Wang et al. [11] utilize sparse signal reconstruction rather than the subspace technique for mixed source localization, which exploits the property that the locations of the point source signals are usually very sparse relative to the entire spatial domain. It achieves high resolution and high estimation accuracy. However, there exists a problem in this method [11] that the range grids set should include both near-field region and far-field region, whether the source is near-field one or far-field one. This will bring considerable computational burden. In addition, this method would fail in the presence of Gaussian sources since it uses fourth-order cumulant [10].

In this paper, we propose a new mixed source localization method jointly using MUSIC and sparse signal representation. The proposed method includes three steps: (i) transform the output data of array into second-order statistics data and obtain the DOA estimation of all sources using the weighted $\ell_1$-norm minimization; (ii) utilize MUSIC spectra function to distinguish the mixed sources and successively obtain a more accurate azimuth DOA estimation of far-field sources; (iii) construct mixed overcomplete matrix and apply it to estimate range parameters of near-field sources. The proposed method is better suited for both Gaussian and Non-Gaussian sources. Compared with the method addressed in [10], the proposed method can provide an improved azimuth DOA and range estimation accuracy of the near-field sources. Moreover, it also performs better in estimating azimuth DOA of far-field sources, as well as range parameters of near-field sources in comparison with the method addressed in [11]. In addition, the computational complexity of the proposed method is much lower than that of [11].

The reminder of this paper is organized as follows: The mixed near-field and far-field signal model based on a symmetric uniform linear array is introduced in Section 2. The mixed source localization method jointly using MUSIC and sparse signal reconstruction is proposed in Section 3. Simulation results are presented in Section 4. Conclusions are drawn in Section 5.

## 2. Mixed near-field and far-field signal model

We consider the data model introduced by Liang and Liu [9] for an array of $2M+1$ sensors receiving $K$ (near-field or far-field)

* Corresponding author. Tel.: +86 431 85095995.
*E-mail address:* tiany11@mails.jlu.edu.cn (Y. Tian).

1434-8411/$ – see front matter © 2014 Elsevier GmbH. All rights reserved.
http://dx.doi.org/10.1016/j.aeue.2013.12.011

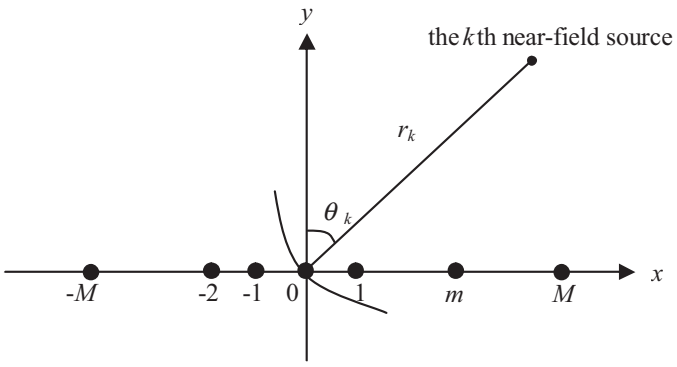


**Fig. 1.** Uniform linear array configuration.

source signals. The array configuration is shown in Fig. 1. Let the array center be the phase reference point. After sampled with a proper rate that satisfies the Nyquist rate, the signal received by the $m$th sensor can be expressed as

$$y_m(t) = \sum_{k=1}^{K} s_k(t) e^{j\tau_{mk}} + n_m(t), \qquad t = 0, \ldots, N-1 \tag{1}$$

where $N$ is the snapshot number, $s_k(t)$ denotes the $k$th source signal, $n_m(t)$ represents the additive Gaussian noise, and $\tau_{mk}$ indicates the delay associated with the $k$th source signal propagation time from 0th to $m$th sensor. If the $k$th source is near-field one, $\tau_{mk}$ can be given by

$$\tau_{mk} = m\gamma_k + m^2\phi_k \tag{2}$$

where $\gamma_k$ and $\phi_k$ are called electric angles and given by

$$\gamma_k = -2\pi \frac{d}{\lambda} \sin(\theta_k) \tag{3}$$

$$\phi_k = \pi \frac{d^2}{\lambda r_k} \cos^2(\theta_k) \tag{4}$$

where $\theta_k$ and $r_k$ are the azimuth DOA and range of the $k$th near-field sources, respectively. $\lambda$ and $d$ denote the carrier wavelength and intersensor spacing, respectively. Otherwise, if the $k$th source is far-field one, $\tau_{mk}$ has the following form:

$$\tau_{mk} = m\gamma_k. \tag{5}$$

Thus, the far-field source can be regarded as a special case of near-field source with $\phi_k = 0$ or $r_k = \infty$.

Consequently, the mixed near-field and far-field signal model can be rewritten as

$$\mathbf{y}(t) = \mathbf{A}\mathbf{s}(t) + \mathbf{n}(t) = \mathbf{A}_N\mathbf{s}_N(t) + \mathbf{A}_F\mathbf{s}_F(t) + \mathbf{n}(t) \tag{6}$$

where $\mathbf{A} = [\mathbf{A}_N\ \mathbf{A}_F]$, $\mathbf{s} = \left[\mathbf{s}_N^T\ \ \mathbf{s}_F^T\right]^T$, and

$$\mathbf{A}_N = [\mathbf{a}_N(\gamma_1, \phi_1), \ldots, \mathbf{a}_N(\gamma_{K_1}, \phi_{K_1})] \tag{7}$$

$$\mathbf{A}_F = [\mathbf{a}_F(\gamma_{K_1+1}), \ldots, \mathbf{a}_F(\gamma_K)] \tag{8}$$

$$\mathbf{a}_N(\gamma_k, \phi_k) = \left[e^{-jM\gamma_k + M^2\phi_k}, \ldots, 1, \ldots, e^{jM\gamma_k + M^2\phi_k}\right]^T \tag{9}$$

$$\mathbf{a}_F(\gamma_k) = [e^{-jM\gamma_k}, \ldots, 1, \ldots, e^{jM\gamma_k}]^T \tag{10}$$

$$\mathbf{s}_N(t) = \left[s_1(t), \ldots, s_{K_1}(t)\right]^T \tag{11}$$

$$\mathbf{s}_F(t) = \left[s_{K_1+1}(t), \ldots, s_K(t)\right]^T \tag{12}$$

where $K_1$ and $K - K_1$ denote the number of near-field sources and far-field sources respectively and the superscript $T$ stands for the transpose operator.

Throughout the rest of the paper, the following assumptions are required:

1. The source signals are statistically independent, zero mean stationary processes.
2. The sensor noise is zero-mean, circular Gaussian, spatially uniformly white and independent from the source signals.
3. The sensor array is a symmetric uniform linear array composed of $2M+1$ sensors. To avoid an ambiguity of phase in mixed sources localization scenario, the inter-element spacing is $d \le \lambda/4$, and the source number is $K < M+1$.

## 3. Proposed method

### 3.1. DOA estimation of all sources

In this paper, second-order statistics is considered. The array covariance matrix is defined as

$$\mathbf{R} = \mathrm{E}\left\{\mathbf{y}(t)\mathbf{y}^H(t)\right\} = \mathrm{AP}\mathbf{A}^H + \sigma^2\mathbf{I} \tag{13}$$

where $\mathbf{P} = \mathrm{E}\left\{\mathbf{s}(t)\mathbf{s}^H(t)\right\} = \mathrm{diag}\{P_1, \ldots, P_K\}$ is the signal covariance matrix, $P_k$ is the power of $k$th signal, $\sigma^2$ is the noise variance, $\mathrm{E}\{\cdot\}$ and $H$ denote the expectation and the conjugate transpose operation, respectively. The symbol $\mathrm{diag}\{z_1, z_2\}$ represents a diagonal matrix with diagonal entries $z_1$ and $z_2$.

Let $r_{p,q}$ be the cross-correlation coefficient of the $p$th and $q$th array output, which is defined by

$$r_{p,q} = \mathrm{E}\left\{y_p(t)y_q^*(t)\right\} \quad = \sum_{k=1}^{K} a_p(\gamma_k, \phi_k)a_q^*(\gamma_k, \phi_k)P_k + \sigma^2\delta_{p,q} \tag{14}$$

where $a_p(\gamma_k, \phi_k)$ is the $(p, k)$th element of $\mathbf{A}$. $\delta_{p,q}$ denotes the Dirac delta function. From (13), we can obtain that the anti-diagonal elements of array covariance matrix $\mathbf{R}$ can be expressed as

$$\mathbf{R}(i, 2M+2-i) = \sum_{k=1}^{K} P_k e^{-j2(M+1-i)\gamma_k} + \sigma^2\delta_{i,2M+2-i} \tag{15}$$

where $i \in [1, 2M+1]$. Therefore, for all $i$, we can form the following $(2M+1) \times 1$ signal model

$$\boldsymbol{\Gamma} = [\mathbf{R}(1, 2M+1), \ldots, \mathbf{R}(2M+1, 1)]^T = \mathbf{B}\mathbf{P} + \sigma^2\mathbf{I}_M \tag{16}$$

where

$$\mathbf{B} = [\mathbf{b}(\theta_1), \ldots, \mathbf{b}(\theta_K)] \tag{17}$$

$$\mathbf{b}(\theta_k) = [e^{-j2M\gamma_k}, e^{-j2(M-1)\gamma_k}, \ldots, 1, \ldots, e^{j2M\gamma_k}]^T \tag{18}$$

$\mathbf{P} = [P_1, \ldots, P_K]^T$ and $\mathbf{I}_M$ is a $(2M+1) \times 1$ vector, whose $M$th element is one and the others are zeros. Assume that the number of sources $K$ is known or correctly estimated by the Akaike information criterion (AIC) or the minimum description length (MDL) detection criterion [12]. Then the noise variance can be obtained by the average of the $2M+1-K$ smallest eigenvalues of $\mathbf{R}$. Consequently, we can obtain a noise-free model

$$\boldsymbol{\Gamma}_1 = \boldsymbol{\Gamma} - \sigma^2\mathbf{I}_M = \mathbf{B}\mathbf{P}. \tag{19}$$

Note that formulation (19) can be considered as a spatial signature of the sources, which is dependent only on the information of DOAs.

In sparse signal representation framework, Eq. (19) can be rewritten as

$$\boldsymbol{\Gamma}_1 = \mathbf{B}_\gamma(\Theta)\mathbf{P}_{\overline{K}} \tag{20}$$

where $\mathbf{B}_\gamma(\Theta) = [\mathbf{b}_\gamma(\tilde{\theta}_1), \ldots, \mathbf{b}_\gamma(\tilde{\theta}_{\overline{K}})]$ is an overcomplete basis matrix. The set $\Theta = \{\tilde{\theta}_1, \ldots, \tilde{\theta}_{\overline{K}}\}$ is a sampling grid of potential directions in spatial domain, $\mathbf{P}_{\overline{K}} = \left[\tilde{P}_1, \ldots, \tilde{P}_i, \ldots, \tilde{P}_{\overline{K}}\right]^T$ is a $K$-sparse vector, whose $i$th element is nonzero and equal to $P_k$ if signal $k$ comes from $\tilde{\theta}_i$ for some $k$ and zero otherwise. In general, $\overline{K} \gg K$.

Subsequently, the DOA estimation of all sources can be obtained by solving the following mixed $\ell_2$–$\ell_1$-norm minimization problem

$$\min\{(1-h)\left\|\boldsymbol{\Gamma}_1 - \mathbf{B}_\gamma \mathbf{P}_{\overline{K}}\right\|_2 + h\left\|\mathbf{P}_{\overline{K}}\right\|_1\} \tag{21}$$

where $\|\cdot\|_2$ and $\|\cdot\|_1$ denote the $\ell_2$-norm and $\ell_1$-norm, respectively. $h$ is a regularization parameter that balances the $\ell_2$-norm term and $\ell_1$-norm term.

As stated in [13], the $\ell_1$-norm penalty is not democratic since it penalizes larger coefficients more heavily than smaller coefficients. This causes the degradation of signal recovery performance. Thus, we propose the weighted $\ell_1$-norm penalty to improve the estimation accuracy.

We divide the vector $\boldsymbol{\Gamma}_1$ into $\overline{L}(>K)$ overlapping subvectors, where each subvector contains $2M+2-\overline{L}(>K)$ elements. Then, we form the $(2M+2-\overline{L}) \times \overline{L}$ matrix

$$\mathbf{y}_1 = \mathbf{B}_1 \mathbf{P}_{\overline{L}} \tag{22}$$

where

$$\mathbf{B}_1 = [\mathbf{b}_1(\theta_1), \ldots, \mathbf{b}_1(\theta_K)] \tag{23}$$

$$\mathbf{b}_1(\theta_k) = [e^{-j2(M+1)\gamma_k}, \ldots, e^{j2(M-\overline{L})\gamma_k}]^T \tag{24}$$

$$\mathbf{P}_{\overline{L}} = [\mathbf{p}_1, \ldots, \mathbf{p}_{\overline{L}}] \tag{25}$$

$$\mathbf{p}_l = [P_1 e^{j2l\gamma_k}, \ldots, P_K e^{j2l\gamma_K}]^T \tag{26}$$

With a total of $\overline{L}$ groups, we can compute the $(2M+2-\overline{L}) \times (2M+2-\overline{L})$ covariance matrix of $\mathbf{y}_1$ as

$$\mathbf{R}_1 = \frac{1}{\overline{L}} \sum_{l=1}^{\overline{L}} \mathbf{B}_1 \mathbf{p}_l \mathbf{p}_l^H \mathbf{B}_1^H. \tag{27}$$

Let $\mathbf{U}_n$ denote the $(2M+2-\overline{L}) \times (2M+2-\overline{L}-K)$ noise-subspace matrix of $\mathbf{R}_1$, which is corresponding to the $(2M+2-\overline{L}-K)$ small singular values, then the weight $\omega_i$ has the following form

$$\omega_i = \mathbf{b}_1^H(\tilde{\theta}_i) \mathbf{U}_n \mathbf{U}_n^H \mathbf{b}_1(\tilde{\theta}_i). \tag{28}$$

If the $\tilde{\theta}_i$ equals to the DOA of a certain source, $\omega_i$ should be small coefficient for orthogonality between $\mathbf{b}_1(\tilde{\theta}_i)$ and $\mathrm{U}_n$. Then, a more accurate DOA estimation can be obtained by the following weighted $\ell_2$–$\ell_1$-norm minimization problem

$$\min\{(1-h)\left\|\boldsymbol{\Gamma}_1 - \mathbf{B}_\gamma \mathbf{P}_{\overline{K}}\right\|_2 + h\sum_{i=1}^{\overline{K}} \omega_i |\tilde{P}_i|\} \tag{29}$$

The optimization problem (29) belongs to convex optimization problem, and can be calculated by SOC software package [14]. Let $\mathbf{P}_{\overline{K}}^0$ be the reconstruction result of (29), then the DOAs can be obtained by finding the index of nonzero coefficients or $K$ larger coefficients in $\mathbf{P}_{\overline{K}}^0$.

As stated by several literatures, the regularization parameter $h$ plays an important role in the final performance. A large $h$ emphasizes the role of the $\ell_1$-term, which may cause wrong source parameter estimation. A small $h$ emphasizes the role of the $\ell_2$-term, which may produce many spurious peaks in spatial spectrum. Here, we exploit the idea of $L$-curve [15] to select $h$ properly. The $L$-curve is a convenient graphical tool for displaying the trade-off between the size of a regularized solution and its fit to the given data, as the regularization parameter varies. According to the theory of the $L$-curve, a plot of $\log\left\|\mathbf{P}_{\overline{K}}\right\|_1$ versus $\log\left\|\boldsymbol{\Gamma}_1 - \mathbf{B}_\gamma \mathbf{P}_{\overline{K}}\right\|_2$ for different values of $h$ will be sharped like an $L$ and that a good choice of value for $h$ is the one corresponding to the corner in the $L$. As shown in Fig. 2, we can easily obtain that the optimal regularization parameter is $h = 0.55$.

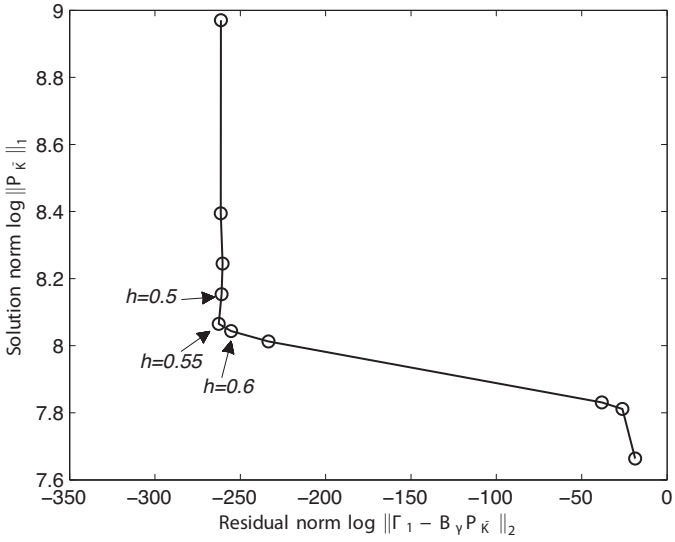


**Fig. 2.** The $L$-curve in the log–log scale.

### 3.2. Classification of the mixed sources and range estimation

Although we have obtained the DOA estimation of all sources, however, the mixed sources are not distinguished up to now. According to the 2D MUSIC algorithm, the 2D spatial spectrum will exhibit exactly $K$ peaks, of which $K-K_1$ peaks corresponding to the far-field sources will appear at $r=\infty$ and $\theta=\theta_k$, $k=1,\ldots,K-K_1$. That is, the DOAs of the far-field sources can be obtained by finding the $K-K_1$ peaks from the following 1D spectrum function

$$f(\theta) = \left[\mathbf{a}_N^H(\theta,\infty)\mathbf{E}_n\mathbf{E}_n^H\mathbf{a}_N(\theta,\infty)\right]^{-1} \tag{30}$$

where $\mathbf{E}_n$ denotes the $(2M+1)\times(2M+1-K)$ noise-subspace matrix. Then, the DOA estimation of far-field sources are obtained, and the mixed sources are also classified by combining the estimation result of the above subsection. In fact, the 1D MUSIC spectra function (30) will provide an improved DOA estimation accuracy of far-field sources than the weighted $\ell_2$–$\ell_1$-norm minimization process (29) due to making full use of array data.

Note that the near-field source is in the Fresnel region, and the range $r$ is in the interval $[0.62\sqrt{D^3/\lambda}, 2D^2/\lambda]$ [10,11] with $D$ representing the array aperture. In order to obtain the range estimation in sparse signal reconstruction framework, we divide the whole range region of near-field source uniformly into $\overline{K}_2$ grids, and a range set is given by $\mathbf{r}_N = [\bar{r}_1, \ldots, \bar{r}_{\overline{K}_2}]$. The sparse representation of (13) can be written as

$$\mathbf{R} = \mathbf{A}_{\hat{\theta},\mathbf{r}}\mathbf{X} + \sigma^2\mathbf{I} \tag{31}$$

where $\mathbf{X}$ is the sparse representation of $\mathbf{P}\mathbf{A}^H$, and

$$\mathbf{A}_{\theta,\mathbf{r}} = \left[\mathbf{A}_{\hat{\theta}_1,\mathbf{r}_N}, \ldots, \mathbf{A}_{\hat{\theta}_{K_1},\mathbf{r}_N}, \mathbf{A}_{\hat{\theta}_{K_1+1},\infty}, \ldots, \mathbf{A}_{\hat{\theta}_K,\infty}\right] \tag{32}$$

$$\mathbf{A}_{\hat{\theta}_{\bar{k}1},\mathbf{r}_N} = \left[\mathbf{a}\left(\theta_{k1},\bar{r}_1\right), \ldots, \mathbf{a}\left(\theta_{k1},\bar{r}_N\right)\right] \tag{33}$$

$$\mathbf{A}_{\hat{\theta}_{k2},\infty} = \mathbf{a}(\theta_{k2},\infty) \tag{34}$$

The noise-free model can also be obtained by subtracting the noise term, i.e.,

$$\mathbf{R}_2 = \mathbf{R} - \sigma^2\mathbf{I} = \mathbf{A}_{\theta,\mathbf{r}}\mathbf{X}. \tag{35}$$

In order to reduce the computational complexity, the singular value decomposition (SVD) form of (35) is

$$\mathbf{R}_{SV} = \mathbf{A}_{\theta,\mathbf{r}}\mathbf{X}_{SV} \tag{36}$$

where $\mathbf{R}_2 = \mathbf{USV}^H$, $\mathbf{R}_{SV} = \mathbf{R}_2\mathbf{VW}_K$, $\mathbf{X}_{SV} = \mathbf{XVW}_K$, $\mathbf{W}_K = [\mathbf{I}_K, \mathbf{0}]$, $\mathbf{I}_K$ and $\mathbf{0}$ denote the $K \times K$ identify matrix and $K \times (2M+1-K)$ zero matrix, respectively. Define $\overline{\mathrm{x}}^{(\ell_2)} = \left[\overline{x}_1^{(\ell_2)}, \ldots, \overline{x}_{\overline{K}_3}^{(\ell_2)}\right]^T$, where $\overline{x}_i^{(\ell_2)}$ denotes the $\ell_2$-norm of the $i$th row of $\mathbf{X}_{SV}$, and $\overline{K}_3 = (K-K_1)\overline{K}_2 + K_1$. Then, the range estimation problem can be formulated as the following weighted $\ell_2$–$\ell_1$-norm minimization.

$$\min\{(1-h)\left\|\mathbf{R}_{SV} - \mathbf{A}_{\hat{\theta}}(r)\mathbf{X}_{SV}\right\|_F^2 + h\sum_{k=1}^{\overline{K}_3}\overline{\omega}_k|\overline{x}_k^{(\ell_2)}|\} \tag{37}$$

where $\|\cdot\|_F$ denotes the Frobenius norm, $\overline{\omega}_k$ is the weight given by

$$\overline{\omega}_k = \mathbf{A}_{\theta,\mathbf{r}}(:,k)^H\mathbf{E}_n\mathbf{E}_n^H\mathbf{A}_{\theta,\mathbf{r}}(:,k) \tag{38}$$

where $\mathbf{A}_{\theta,\mathbf{r}}(:,k)$ is the $k$th column of $\mathbf{A}_{\theta,\mathbf{r}}$. Obviously, the range parameters of sources can be obtained by solving the optimization problem (37). If the estimated range $\hat{r}_k$ falls into the set $\mathbf{r}_N$, the range parameter corresponds to the near-field sources with DOA $\hat{\theta}_k$, on the contrary, let $\hat{r}_k$ be $\infty$ and the sources lies in the far-field region.

### 3.3. Computational complexity

Regarding the computational complexity, we consider the major part. The method addressed in [11] constructs one $(2M+1)\times(2M+1)^2$-dimensional cumulant matrix and implements the SVD of one $(2M+1)\times(2M+1)^2$-dimensional cumulant matrix and one $(2M+1)\times N$ array time-domain output matrix, which requires $O\{9(2M+1)^3N + 4/3(2M+1)^5 + 4/3(2M+1)N^2\}$. The corresponding sparse signal recovery process with weighted $\ell_1$-norm penalty requires $O\left\{K^3\overline{K}^3 + K^6(\overline{K}_2+\overline{K}_4)^3\right\}$, where $\overline{K}_2$ and $\overline{K}_4$ denote the number of grids of near-field region and far-field region, respectively. However, for the proposed algorithm, we construct one $(2M+1)\times(2M+1)$-dimensional and one $(2M+2-\overline{L})\times(2M+2-\overline{L})$-dimensional second-order statistics matrix, and implements their eigen-decompositions, which requires $O\{(2M+1)^2N + (2M+2-\overline{L})^2\overline{L} + 4/3(2M+1)^3 + 4/3(2M+2-\overline{L})^3\}$. The corresponding sparse signal reconstruction process requires $O\left\{\overline{K}^3 + K^3\overline{K}_3^3\right\}$. Therefore, the computational complexity of the proposed method is much lower than that of [11]. Note that the main complexity of the method addressed in [10] is in calculating the array covariance matrix and its eigenvalue decomposition, which is lower than the proposed method. However, it should be stressed that the proposed method can provide an improved DOA and range estimation of near-field sources.

## 4. Simulations

In this section, the performance of the proposed algorithm is verified by numerical simulations, and is also compared with the method addressed in [10] and [11]. A 9-element symmetric ULA with element spacing $d = \lambda/4$ is considered. The additive noise is assumed to be spatial white complex Gaussian, and the SNR of the $k$th signal is defined as $10\log(P_k/\sigma^2)$. The array covariance matrix $\mathbf{R}$ is estimated through $N$ snapshots as $\mathrm{R} = (1/N)\sum_{t=1}^{N}\mathbf{y}(t)\mathbf{y}^H(t)$. The

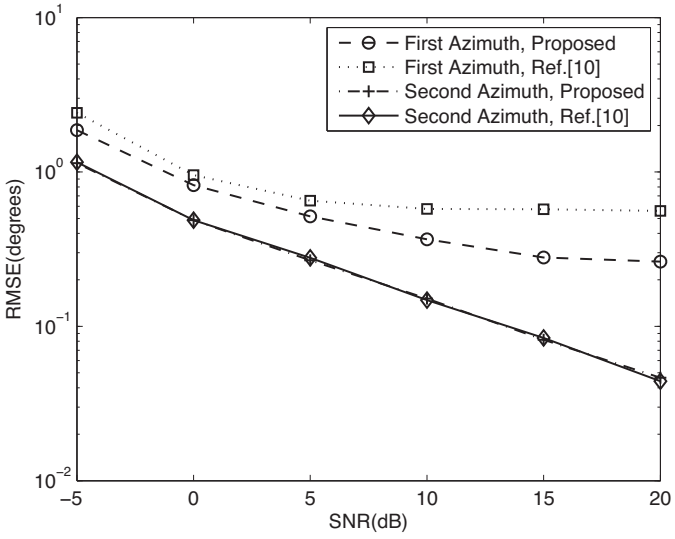


**Fig. 3.** The RMSE of azimuth DOA estimations for mixed sources using the method of [10] and the proposed method versus SNR.

direction grid is initially set to have 181 points sampled from $-90^\circ$ to $90^\circ$ with $1^\circ$ interval, while the range grid is set in the Fresnel region of array with $0.05\lambda$ resolution. The adaptive grid refinement strategy is adopted to alleviate the limitation of the direction and range grid. The regularization parameter $h$ is set to be 0.55. The root mean square error (RMSE) that indicates the performance of the proposed algorithm is obtained by 500 independent Monte-Carlo simulations.

In the first experiment, we compare the RMSE of the DOA and range estimation versus SNR, whose curves are plotted in Figs. 3 and 4, respectively. Two sources located at $\{\theta_1 = 10^\circ, r_1 = 2, 5\lambda\}$ and $\{\theta_2 = 25^\circ, r_2 = \infty\}$ are considered. The source signals are assumed to be uncorrelated Gaussian signals. The number of snapshots is fixed at 200, while the SNR is varied from $-5$ dB to 20 dB in 5-dB steps. From the simulation results, we observe that the estimation accuracy of azimuth DOA of source 2 (far-field source) is same since the same operation is adopted. However, the proposed method can provide a higher estimation accuracy than the method addressed

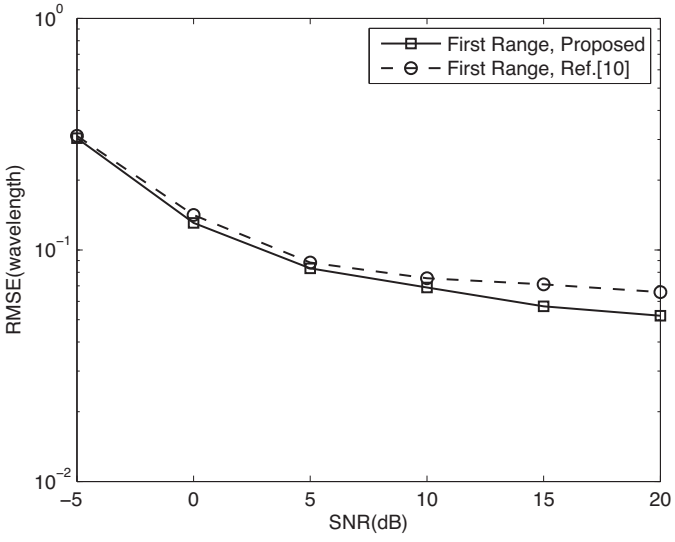


**Fig. 4.** The RMSE of range estimations for mixed sources using the method of [10] and the proposed method versus SNR.

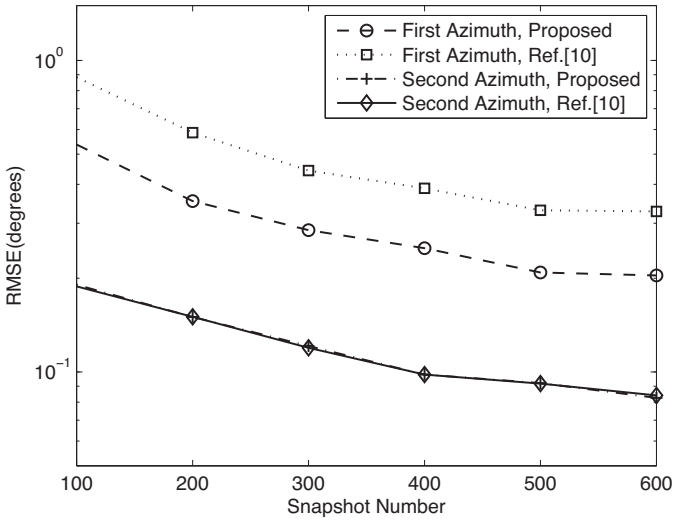


**Fig. 5.** The RMSE of azimuth DOA estimations for mixed sources using the method of [10] and the proposed method versus snapshot number.

in [10] in estimating the azimuth DOA and range of the near-field source.

In the second experiment, we examine the performance of the azimuth and range estimations versus the number of snapshots. The simulation condition is similar to the first example except that the SNR is fixed at 10 dB, and the snapshot number is varied from 100 to 600. As can be seen in Figs. 5 and 6, the estimation performance of near-field source azimuth DOA and range is better than that of [10]. In addition, it is obvious that the RMSE decreases monotonically with the number of snapshots.

In the last experiment, the proposed method is used for the parameter estimation problem when both far-field and near-field non-Gaussian signals present. The simulation condition is again similar to the first experiment except that the two source signals are assumed to be equal-power complex sinusoidal ones. From Figs. 7 and 8, we can conclude that the proposed method not only has a higher estimation accuracy than the method addressed in [10] in estimating the azimuth DOA and range of the near-field source, but also displays a more satisfactory performance in estimating the azimuth DOA of far-field source and the range of near-field

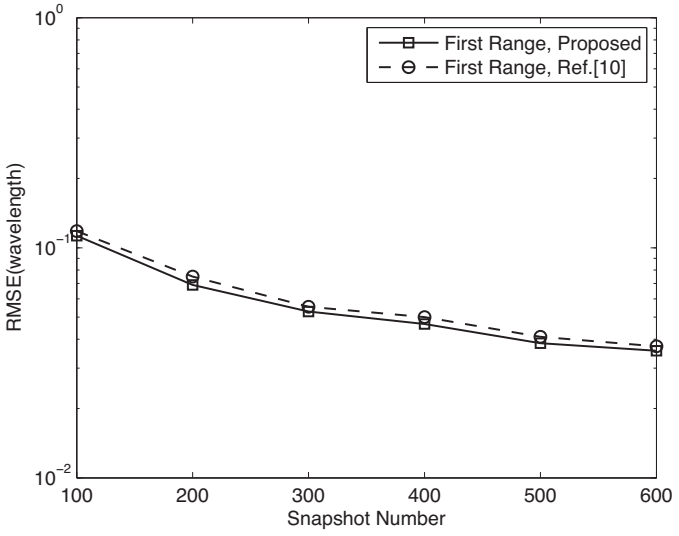


**Fig. 6.** The RMSE of range estimations for mixed sources using the method of [10] and the proposed method versus snapshot number.

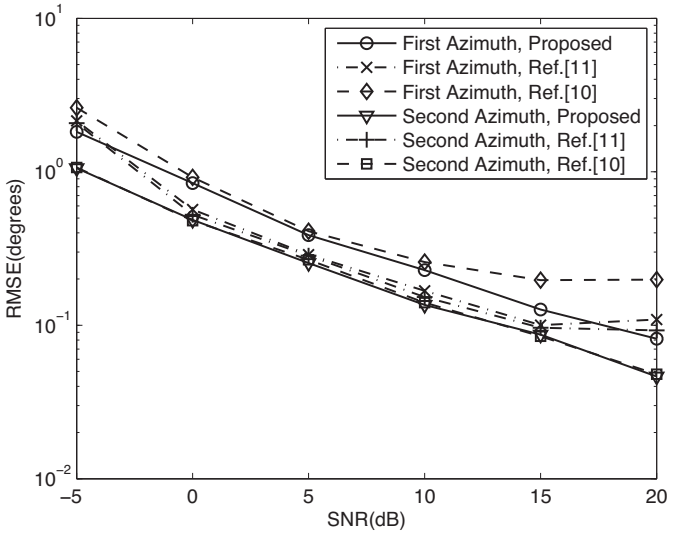


**Fig. 7.** The RMSE of azimuth DOA estimations for mixed sources using the proposed method and that of [10] and [11] versus SNR.

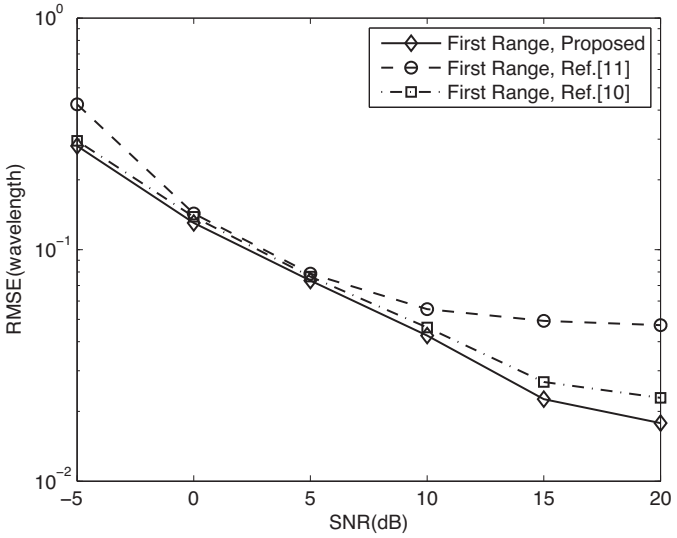


**Fig. 8.** The RMSE of range estimations for mixed sources using the proposed method and that of [10] and [11] versus SNR.

source than the method addressed in [11]. In addition, it should be stressed that our proposed method has lower computational complexity than that of [11].

## 5. Conclusion

In this paper, we propose a new mixed source localization method jointly using MUSIC and sparse signal reconstruction. In this scheme, we firstly transform the time-domain data of array into second-order statistics domain data to estimate the DOAs of all sources using weighted $\ell_1$-norm penalty, then utilize the MUSIC spectra function to distinguish the mixed sources as well as obtain a more accurate azimuth DOA estimation of far-field sources. Finally, we construct the mixed overcomplete basis to get the sparse representation of the array output for range estimation. The simulation results demonstrate the effectiveness and efficiency of the new method.

## Acknowledgments

This paper is supported by the National Nature Science Foundation of China (Grant No: 61171137) and 2009 New Century Excellent Talents in University (NCET-09-0426) in China.

## References

[1] Krim H, Viberg M. Two decades of array signal processing research: the parameter approach. IEEE Trans Signal Process 1996;13:67–94.
[2] Schmidt RO. Multiple emitter location and signal parameter estimation. IEEE Trans Antennas Propag 1986;34:276–80.
[3] Roy R, Kailath T. ESPRIT-estimation of signal parameters via rotational invariance techniques. IEEE Trans Acoust Speech Signal Process 1989;37:984–95.
[4] Yung-Dar H, Barket M. Near-field multiple source localization by passive sensor array. IEEE Trans Antennas Propag 1991;39:968–75.
[5] Yuen N, Friedlander B. Performance analysis of high-order ESPRIT for localization of near-field sources. IEEE Trans Signal Process 1998;46:709–19.
[6] Starer D, Nehorai A. Passive localization of near-field sources by path following. IEEE Trans Signal Process 1994;42:677–80.
[7] Arslan G, Sakarya FA, Evans BL. Speaker localization for far-field and near-field wideband sources using neural networks. In: Proc. IEEE-EURASIP Workshop on Nonlin. Signal Process. 1999. p. 528–32.
[8] Argentieri S, Danes P, Soueres P. Modal analysis based beamforming for nearfield or farfield speaker localization in robotics. In: Proc. 2006 IEEE Int. Conf. Robots Syst. 2006. p. 866–71.
[9] Liang J, Liu D. Passive localization of mixed near-field and far-field sources using two-stage music algorithm. IEEE Trans Signal Process 2010;58:108–20.
[10] He J, Swamy MNS, Ahmad MO. Efficient application of MUSIC algorithm under the coexistence of far-field and near-field sources. IEEE Trans Signal Process 2012;60:2066–70.
[11] Wang B, Liu J, Sun X. Mixed sources localization based on sparse signal reconstruction. IEEE Signal Process Lett 2012;19:487–90.
[12] Wax M, Kailath T. Detection of signals by information theoretic criteria. IEEE Trans Acoust Speech Signal Process 1985;ASSP-33:387–92.
[13] Zheng C, Li G, Zhang H, Wang X. An approach of DOA estimation using noise subspace weighted minimization. In: Proc. IEEE Int. Conf. Acoust., Speech, Signal Process. (ICASSP). 2011. p. 2856–9.
[14] Sturm JF. Using SeDuMi 1.02, a MATLAB toolbox for optimization over symmetric cones. Optim Methods Softw 1999;11:625–53.
[15] Hansen PC, O'Leary DP. The use of the *L*-curve in the regularization of discrete ill-posed problems. SIAM J Sci Comput 1993;14:1487–503.